POLYAMIDE NANOCOMPOSITES FOR SELECTIVE LASER SINTERING

J. H. Koo[1*], S. Lao[1], W. Ho[1], K. Ngyuen[1], J. Cheng[1], L. Pilato[2], G. Wissler[2], and M. Ervin[2]

[1]The University of Texas at Austin, Department of Mechanical Engineering-C2200, Advanced Manufacturing Center, Austin, TX 78712-0292

[2]KAI, Inc., Austin, TX 78739

[*]Corresponding author: jkoo@mail.utexas.edu

ABSTRACT

Current polyamide 11 and 12 are lacking in fire retardancy and high strength/high heat resistance characteristics for a plethora of finished parts that are desired and required for performance driven applications. It is anticipated that nanomodification of polyamide 11 and 12 will result in enhanced polymer performance, i.e., fire retardancy, high strength and high heat resistance for polyamide 11 and 12. It is expected that these findings will expand the market opportunities for polyamide 11 and 12 resin manufacturers.

The objective of this research is to develop improved polyamide 11 and 12 polymers with enhanced flame retardancy, thermal, and mechanical properties for selective laser sintering (SLS) rapid manufacturing (RM). A nanophase was introduced into the polyamide 11 and 12 via twin screw extrusion to provide improved material properties of the polymer blends. Arkema RILSAN® polyamide 11 molding polymer pellets and Degussa VESTAMID® L1670 polyamide 12 were examined with three types of nanoparticles: chemically modified montmorillonite (MMT) organoclays, surface modified nanosilica, and carbon nanofibers (CNFs) to create polyamide 11 and 12 nanocomposites.

Wide angle X-ray diffraction (WAXD) and transmission electron microscopy (TEM) were used to determine the degree of dispersion. Injection molded test specimens were fabricated for physical, thermal, mechanical properties, and flammability tests. Thermal stability of these polyamide 11 and 12 nanocomposites was examined by TGA. Mechanical properties such as tensile, flexural, and elongation at break were measured. Flammability properties were also obtained using the Cone Calorimeter at an external heat flux of 50 kW/m^2. TEM micrographs, physical, mechanical, and flammability properties are included in the paper. Polyamide 11 and 12 nanocomposites properties are compared with polyamide 11 and 12 baseline polymers. Based on flammability and mechanical material performance, selective polymers including polyamide 11 nanocomposites and control polyamide 11 were cryogenically ground into fine powders and fabricated into SLS parts.

INTRODUCTION

Flame retardant (FR) additives, including inorganic metal oxides/hydroxides or halogens with or without phosphorous and nitrogen containing materials, are required in conventional methods to modify flammable thermoplastic materials to FR products [1].

Large amounts of FR additives (>30%) are necessary in those methods to make FR thermoplastics. In many cases, it results in a reduction of mechanical properties, such as toughness, melt flow, etc. and/or release of smoke and toxic emissions when the modified thermoplastic is burning.

Nanotechnology allows nanoparticles to be incorporated into the thermoplastic by twin-screw extrusion (a melt blending process) to develop new FR thermoplastic polymer. A low amount of nanoparticles (<7%) is required by such method to make nanocomposites that exhibit similar enhanced flammability properties when compared with the modified thermoplastic processed by conventional methods [2-12]. Nevertheless, unlike the conventional FR thermoplastic resins, the resulting nanocomposites exhibit enhanced mechanical properties such as high strength/modulus, moisture resistance, higher heat deflection temperature, etc. Therefore, this technology can be used to develop novel thermoplastic structural components with high performance and fire resistance.

The major technical objective of this study was to investigate the relationship between the enhanced mechanical and flammability properties of selected polyamide 11 and 12 nanocomposites and their microstructures using SEM and TEM. Different types of nanoparticles were melt blended with Arkema RILSAN® PA11 and Degussa Vestamid® L1670 polyamide 12 to form polyamide 11 nanocomposites (PA11N) and polyamide 12 nanocomposites (PA11N), respectively. The nanoparticles used were: (a) surface-modified nanoclays, (b) surface-modified nanosilicas, and (c) carbon nanofibers (CNF).

2. EXPERIMENTAL

2.1 Materials

Polymer Resin Polyamides (PA) are versatile thermoplastic engineering polymeric materials noted for outstanding properties such as high tensile strength, good resistance to flow under pressure (creep), excellent abrasion, chemical and heat resistance, and a low coefficient of friction. Polyamides such as PA6 and PA66 are high melting, moderately crystalline polymers (T_m 220-265°C) while PA11 and PA12 are intermediate melting materials (<200°C) and are less susceptible to moisture as compared to PA6 and PA66. Paul *et al.* [13] have examined the structure and properties of nanocomposites based on PA6, PA11, and PA12. Their studies were restricted to nanoclays whereas our studies are directed to examining/comparing nanoclay and other nanoparticles to determine enhanced polymer characteristics such as flame retardancy and improved thermal/mechanical properties for the resulting PA11N and PA12N.

Arkema's RILSAN® polyamide 11 (PA11) thermoplastic material was selected for this study since it is an attractive polyamide used in quite a diversity of applications. RILSAN® PA11 thermoplastic [14] is a high-performance polymer developed by Atofina Chemicals, Inc. in 1942. Derived from a series of complex chemical operations, RILSAN® PA11 is one of the few polymers in existence produced from a 'green' raw materials – castor beans. RILSAN® PA11 resin has earned a preferred material status in the most demanding applications due largely to their unique combination of thermal, physical, chemical, and mechanical properties. This results in an outstanding Cost Performance Ratio. Processing ease is another major benefit of RILSAN® polyamide 11

resins. Supplied in powder or pellet form RILSAN® PA11 PCGLV resin can be processed by injection molding, extrusion, blown film extrusion, extrusion blow molding or rotomolding. RILSAN® PA11 resin has a unique combination of properties.

Degussa's Vestamid® L1670 polyamide 12 (PA12) thermoplastic material was selected for this study since it is also an attractive polyamide used in many diverse applications. Vestamid® PA12 thermoplastic [15] is a high-performance polymer developed by Degussa in 1963. Vestamid® L1670 is a heat-stabilized and unreinforced PA12 with low viscosity and natural color appearance. The polyamide 12 resin has superior properties such as low density, high toughness, impermeability and very good chemical resistance, high abrasion resistance, noise and vibration damping, etc. Processing ease is another major benefit of Vestamid® polyamide 12 resins. Available in powder or pellet form Vestamid® PA12 resin can be processed by injection molding, extrusion, blown film extrusion, extrusion blow molding or rotomolding.

Nanoparticles Three types of nanoparticles were used, namely Southern Clay Products' montmorillonite (MMT) nanoclays, Degussa's nanosilica, and Applied Sciences' carbon nanofibers (CNF). A brief discussion of these nanoparticles is included in this section for completeness; more detailed description of these nanopraticles can be found in a recent book by Koo [16]. These nanoparticles will reinforce the polymer in the nanoscale and will enhance the dimensional stability and mechanical properties of the polymer nanocomposites. To achieve the potential improvements it usually requires excellent dispersion and some degree of exfoliation (for nanoclay). These are shown to be dependent upon a combination of proper chemical treatment and optimized processing.

Nanoclays Achieving exfoliation of organomontmorillonite in various continuous phases is a function of the surface treatment of the MMT clays and the mixing efficiency of the dispersing protocol. Surface treatment of MMT is classically accomplished with the exchange of inorganic counterions, e.g., sodium etc., with quaternary ammonium ions. Two MMT nanoclays including Southern Clay Products (a) Cloisite® 30B (a natural MT modified with an organic modifier, MT_2EtOT: methyl-tallow-bis-2-hydroxyethyl-quaternary ammonium at 90 meq/100g) [16, 17] and (b) Cloisite® 93A (a natural MMT modified with an organic modifier M_2HT: methyl-dihydrogenated tallow ammonium at 90 meq/100g clay) [16, 18] were selected.

Nanosilica AEROSIL® is highly dispersed, amorphous, very pure silica that is produced by high-temperature hydrolysis of silicon tetrachloride in an oxyhydrogen gas flame [16, 19-21]. The primary particles are spherical and free of pores. The primary particles in the flame interact to develop aggregates that join together reversibly to form agglomerates. AEROSIL® 300 is a hydrophilic fumed silica with a specific surface of 300 m^2/g manufactured by Degussa. It has an average particle size of 7 nm in diameter. AEROSIL® fumed silica for rheology control is widely used in silicone rubber, coatings, plastics, printing inks, adhesives, lubricants, creams, ointment, and in toothpaste.

Carbon Nanofibers (CNF) CNF are a form of vapor-grown carbon fiber, which is a discontinuous graphitic filament produced in the gas phase from the pyrolysis of hydrocarbons [16, 22-24]. It bridges the gap in physical properties between larger, conventional PAN or pitch-based carbon fibers (5 – 10 μm) and smaller single-wall and multi-wall carbon nanotubes (1 – 10 μm). In properties of physical size, performance improvements, and product cost, CNF complete a continuum bounded by carbon black,

fullerenes, and single-wall to multi-wall carbon nanotubes on one end and continuous carbon fiber on the other end. PR-19-PS CNF was used in our study.

The morphology of selective resin/nanoparticle systems was characterized using TEM and SEM analyses. These TEM images facilitated screening various formulations for desirable nano-level dispersion of the clay, nanosilica, or CNF within the polymer. Desirable features included higher levels of clay exfoliation, nanodispersion of nanosilica, and uniform dispersion of CNF within the polymer.

2.2 Measurements

Thermal Stability Testing Thermal stability of the PA12 baseline and PA12N was examined by thermogravimetric analysis (TGA) using the Perkin Elmer TGA 7. Weight changes in sample materials are measured as a function of temperature or time in TGA. The sample is heated by a furnace under nitrogen while the loss or gain of sample weight due to chemical reactions, decomposition, solvent or water evaporation, Curie point transitions and oxidation is monitored by a sensitive balance. Weight, temperature, and furnace calibrations were carried out for the usable range of the TGA (100-900°C) at a scan rate of 20°C/min.

Mechanical Testing In order to compare the mechanical properties of the nanocomposites polyamide 11 and 12 with the baseline materials, stress-strain behavior was performed using an automated tensile testing system (Instron model 4301). Tensile strength, flexural strength, Young's modulus, and elongation at break were obtained from the stress-strain data. Tensile tests (ASTM D638) measure the force required to break a specimen and the extent to which the specimen stretches or elongates to that breaking point. Tensile tests produce a stress-strain diagram, which is used to determine tensile modulus. Since the physical properties of many materials (especially thermoplastics) can vary depending on ambient temperature, it is sometimes appropriate to test materials at temperatures that simulate the intended end use environment. The polyamide 11 and 12 nanocomposite specimens were tested using an automated tensile testing system (Instron model 1137).

Flammability Testing The tests described herein were conducted in accordance with ASTM E1354 standard test method for heat and visible smoke release rates for materials and products using an oxygen consumption calorimeter. The method is based on the observation that the net heat of combustion of most materials is directly related to the amount of oxygen required for released per kilogram of oxygen consumed. Specimens in the test are burned in ambient air conditions, while being subjected to a predetermined external heat flux and set from 0 to 100 kW/m^2. A heat flux of 50 kW/m^2 was utilized in our study. The primary measurements are oxygen concentration and exhaust gas flow rate. Additional measurements include the mass loss rate of the specimen, the time to sustained flaming, release rates of carbon monoxide and carbon dioxide, and smoke obscuration.

3. RESULTS AND DISCUSSION

3.1 Processing and Characterization of Resin/Nanoparticle Systems

Processing and characterization of PA11-nanoclay, PA11-nanosilica, and PA11-carbon nanofibers, PA12-nanoclay, and PA12-carbon nanofibers are discussed briefly in this section.

Blending Nanoclays/PA11 Polymer Chemically treated pillared clays such as Cloisite® 30B and 93A organoclays were used. The individual clay layers are separated by alkyl ammonium ion incorporation (d spacing increased) allowing for possible intercalation of solid organic resins if the clay is melt blended with the resins. Clays were blended with the PA11 resin to intercalate and eventually exfoliate the resin within the clay layers. Twin screw extrusion mixing should enhance the exfoliation rate. The degree of exfoliation was estimated by wide angle X-ray diffraction (WAXD) and TEM.

A 30 mm Werner Pfleider corotating twin screw extruder which is configured for a wide variety of materials was used. The extruder L/D can be varied from 21 to 48, with options of multiple feeds and vents. The energy profile of the screw is adjusted to optimally meet the needs of the target product. Long residence time screw designs are available for reactive products. A variety of feeders are available to accommodate the material handling characteristics of the raw materials. Strand pelletization with low temperature chilled fluids allows processing of very soft or rubbery materials.

Table 1 shows the two nanoclays selected at 2.5, 5, 7.5, and 10 wt% loading levels with the PA11 resin. For the clay, the screw profile was set for a relatively long residence time for high shear characteristics to allow for complete separation of the nanoclays and full dispersion into the polymer matrix. Approximately 10 lbs of each formulation were produced. Separate volumetric feeders were used for the base resin and the nanoparticles. The PA11 was dried in a desiccant drier before compounding. Injection molded specimens of each blend were prepared and examined by WAXD and TEM. Figure 1 shows the TEM micrographs of the 90% PA11:10% Cloisite® 30B. It is evident that exfoliation of Cloisite® 30B in PA11 polymer was achieved.
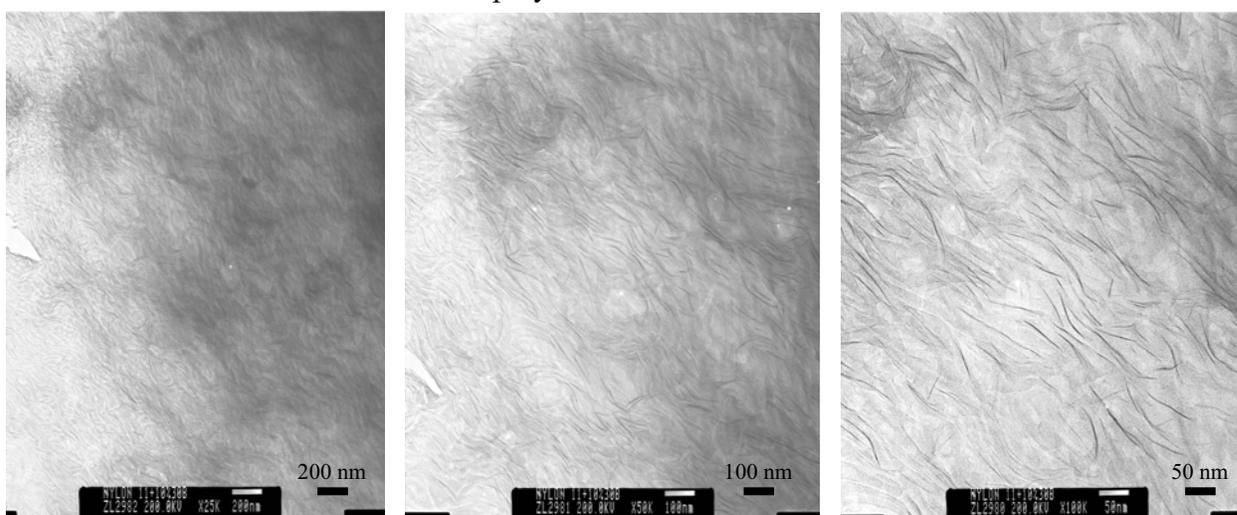
Figure 1 TEM micrographs of the 90% PA11:10% Cloisite 30B polymer showing exfoliation of nanoclay in PA11 was achieved.

Table 1 Material Matrix for Polyamides/Nanoparticles

SAMPE NO.	RESIN (WT PERCENT)	NANOPARTICLES (WT PERCENT)	NANOPARTICLES TYPE
1	PA11 100%	0%	None
2	PA11 97.5%	2.5%	Cloisite® 30B
3	PA11 95%	5.0%	Cloisite® 30B
4	PA11 92.5%	7.5%	Cloisite® 30B
5	PA11 90%	10%	Cloisite® 30B
6	PA11 97.5%	2.5%	Cloisite® 93A
7	PA11 95%	5.0%	Cloisite® 93A
8	PA11 92.5%	7.5%	Cloisite® 93A
9	PA11 90%	10%	Cloisite® 93A
10	PA11 99%	1.0%	PR-19-PS CNF
11	PA11 97%	3.0%	PR-19-PS CNF
12	PA11 95%	5.0%	PR-19-PS CNF
13	PA11 93%	7.0%	PR-19-PS CNF
14	PA11 97.5%	2.5%	Aerosil® 300
15	PA11 95%	5.0%	Aerosil® 300
16	PA11 92.5%	7.5%	Aerosil® 300
17	PA12 100%	0%	None
18	PA12 97.5%	2.5%	Cloisite® 30B
19	PA12 95%	5.0%	Cloisite® 30B
20	PA12 92.5%	7.5%	Cloisite® 30B
21	PA12 97%	3.0%	PR-19-PS CNF
22	PA12 95%	5.0%	PR-19-PS CNF
23	PA12 93%	7.0%	PR-19-PS CNF

Blending Carbon Nanofibers/PA11 Polymer PR-19-PS CNF is about 130 nm in diameter and several microns in length, and can be classified as MWNT. It was blended with PA11 polymer in four different loading levels via twin screw extrusion. Table 1 shows that the CNF was selected at 1, 3, 5, and 7 wt% loading levels with the PA11 resin. For the CNF, the screw was configured to allow separation of the CNF without fracturing them.
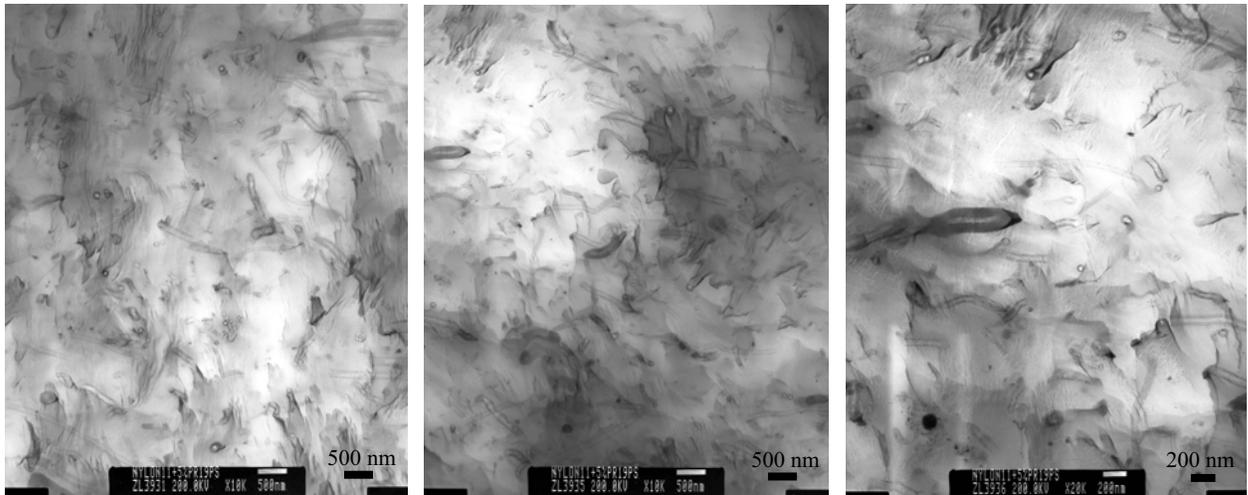
Figure 2 TEM micrographs of the 95% PA11:5% PR-19-PS polymer showing good dispersion of CNF in PA11 was achieved.

Approximately 10 lbs of each formulation were produced. Injection molded specimens of each blend were prepared and examined by TEM as shown in Figure 2. It is evident good dispersion of PR-19-PS CNF in PA11 was achieved.

Blending Nanosilicas/PA11 Polymer Nanosilica Aerosil® 300 was blended with PA11 polymer in three different loading levels. Table 1 shows that the nanosilica was selected at 2.5, 5, and 7.5 wt% loading levels with the PA11 resin. For the nanosilica, the screw profile was set at a relatively long residence time for high shear characteristics to allow for complete separation of the nanosilicas and full dispersion into the polymer matrix. Approximately 10 lbs of each formulation were produced. Injection molded specimens of each blend were prepared and examined by TEM as shown in Figure 3. It is evident that very large aggregates (micron size) of nanosilica were formed. Nanosilica could not be uniformly dispersed into PA11 and was not attempted with PA12.
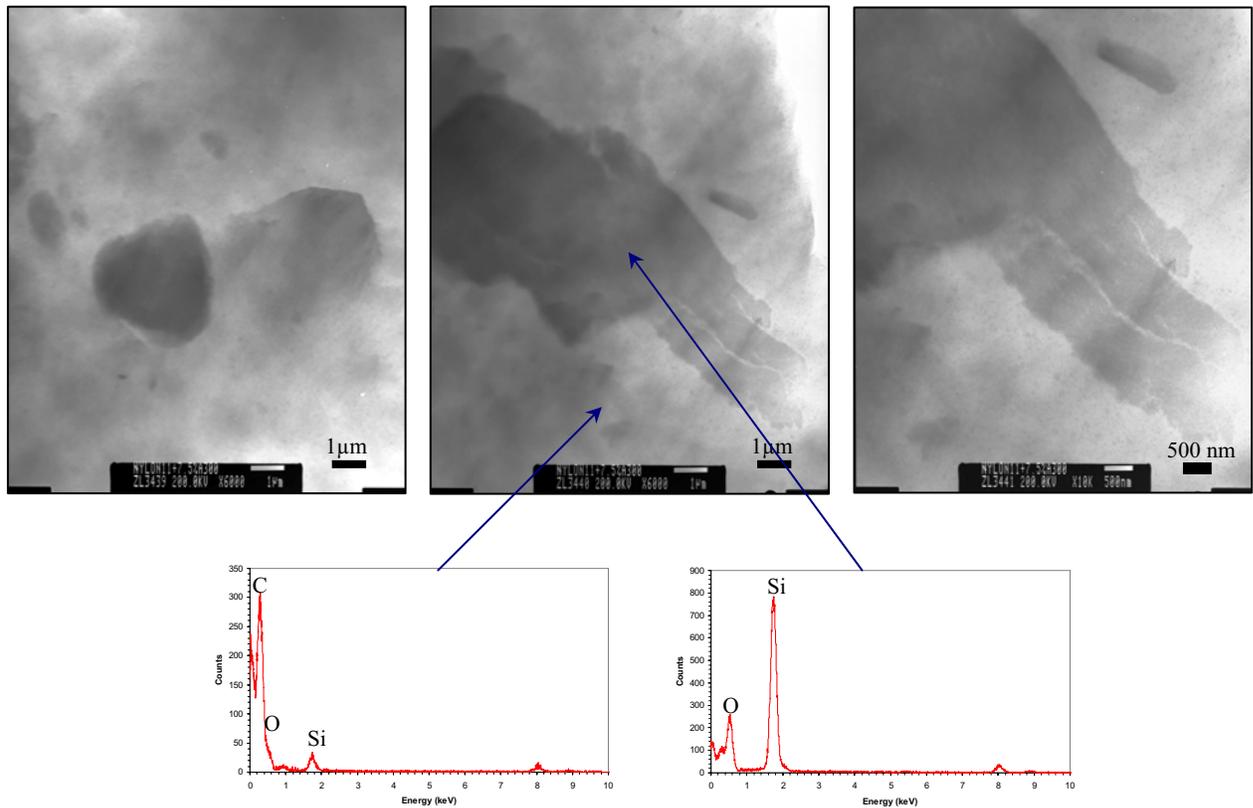
Figure 3 TEM micrographs of the 92.5% PA11:7.5% Aerosil® 300 nanosilica polymer showing very large nanosilica aggregates were formed in the PA11 polymer.

Blending Nanoclays/PA12 Polymer Chemically treated pillared clays Cloisite® 30B organoclay was used. The individual clay layers are separated by alkyl ammonium ion incorporation (d spacing increased) allowing for possible intercalation of solid organic resins if the clay is melt blended with the resins. Clay was blended with the PA12 polymer to intercalate and eventually exfoliate in the resin. Twin screw extrusion should enhance the exfoliation rate. The degree of exfoliation was estimated by wide angle X-ray diffraction (WAXD) and TEM. The PA12 was dried in a desiccant drier before compounding. Injection molded specimens of each blend were prepared and examined by

WAXD and TEM. Table 1 shows that the nanoclay was selected at 2.5, 5, and 7.5 wt% loading levels with the PA12 resin. Figure 4 shows the TEM micrographs of the 97.5% PA12:2.5% Cloisite® 30B in progressive magnifications from left to right. It is evident that exfoliation of Cloisite® 30B in PA12 polymer was achieved.
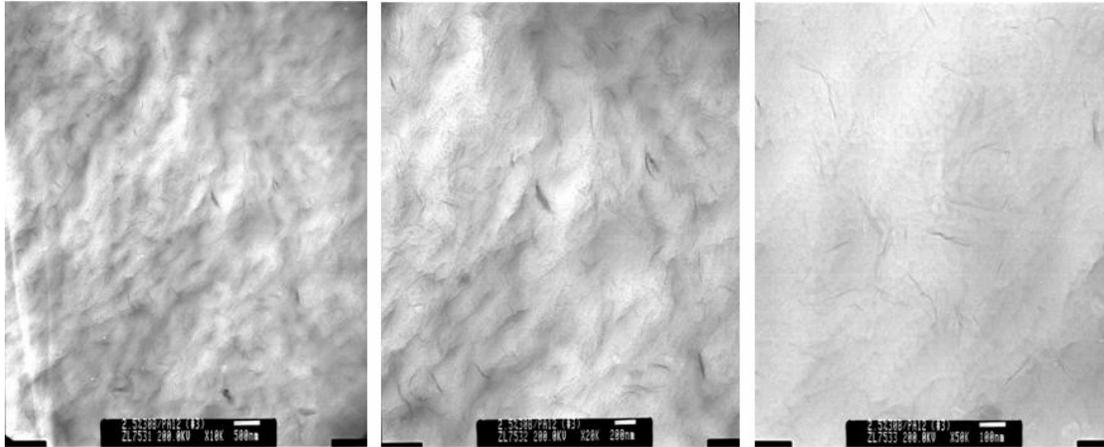
Figure 4 TEM micrographs of the 97.5% PA12:2.5% Cloisite 30B polymer.

Blending Carbon Nanofibers/PA12 Polymer PR-19-PS CNF was blended with PA12 polymer in three different loading levels via twin screw extrusion. Table 1 shows that the CNF was selected at 3, 5, and 7 wt% loading levels with the PA12 resin. For the CNF, the screw was configured to allow separation of the CNF without fracturing them. Approximately 10 lbs of each formulation were produced. Injection molded specimens of each blend were prepared and examined by TEM as shown in Figure 5. It is evident good dispersion of PR-19-PS CNF in PA12 was achieved.
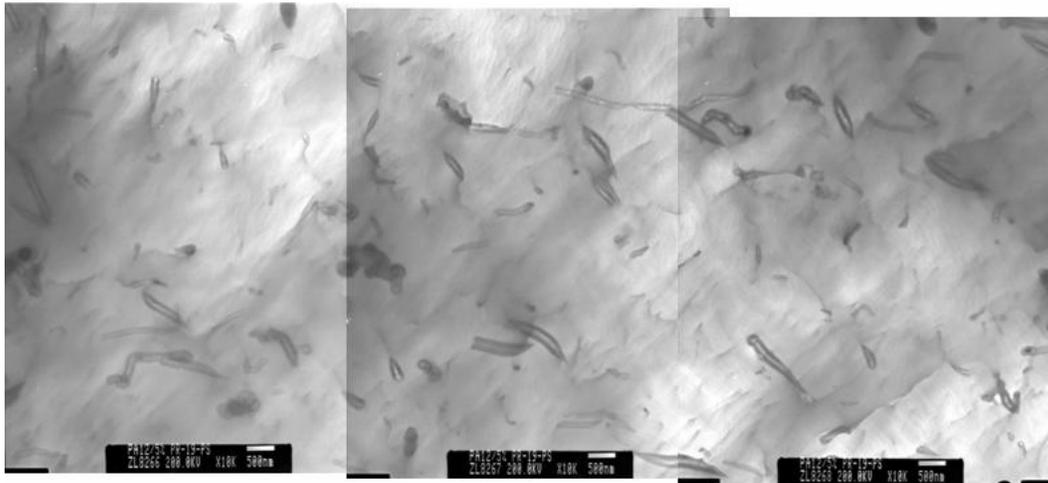
Figure 5 TEM micrographs of the 95% PA12:5% PR-19-PS polymer.

3.2 Thermal Stability and Flammability Properties Resin/Nanoparticle Systems

Figure 6 shows the thermogravimetric analysis (TGA) of the polyamide 12 and the nanocomposite materials. The change of sample weight was measured as a function of temperature. The decomposition temperatures of the PA12-Cloisite® 30B were observed

to be higher than that of the neat PA12 material, while the PA12-carbon nanofibers were about the same as the neat resin system. Our previous study of the microstructures of nylon 11 nanocomposites [25] showed that the clay enhanced the flame resistance properties of the polymer composites. This was achieved by reinforcing the fragile polymer char and forming a protective heat shield (ceramic) layer that blocked the thermal wave from penetrating into the surface. This char reinforcing mechanism may also have contributed to the enhancement in the thermal stability of the polyamide-clay nanocomposites. On the other hand, the char of the burnt nylon 11-CNF was fragile and appeared to burn throughout the polymer matrix. This may be the reason why little or no improvement in the thermal stability of the polyamide 12-CNF nanocomposites was observed.
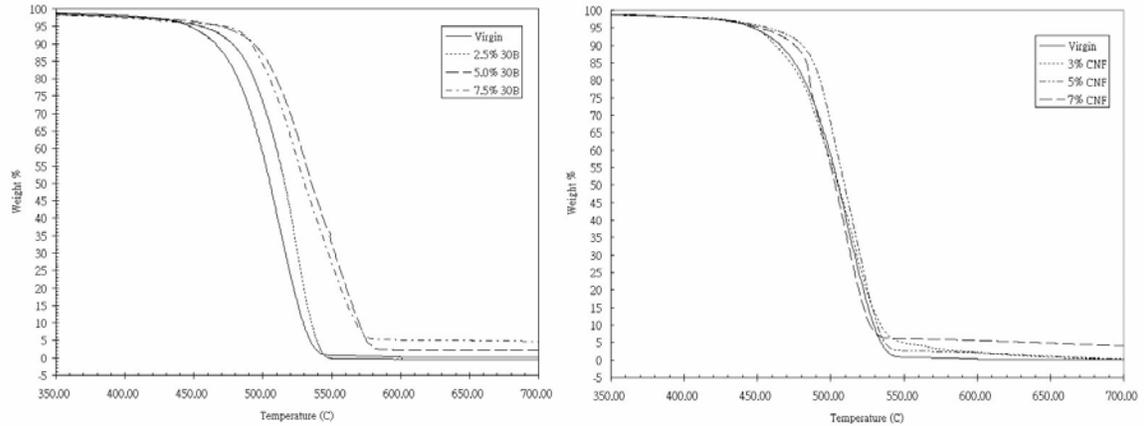
Figure 6 Thermogravimetric analysis of PA12-Cloisite® 30B nanocomposites (left) and PA12-PR-19-PS nanocomposites (right).

Since the flammability properties of baseline PA12 are similar to those of PA11 and based on our previous studies on PA11 clay nanocomposites and PA11 CNF nanocomposites [26], only PA12-5% 30B and PA12-5% CNF were selected for the flammability testing. The following cone calorimeter data were obtained: carbon monoxide emission, instantaneous and peak heat release rate, smoke extinction coefficient, and residual mass (Figures 7 to 10).
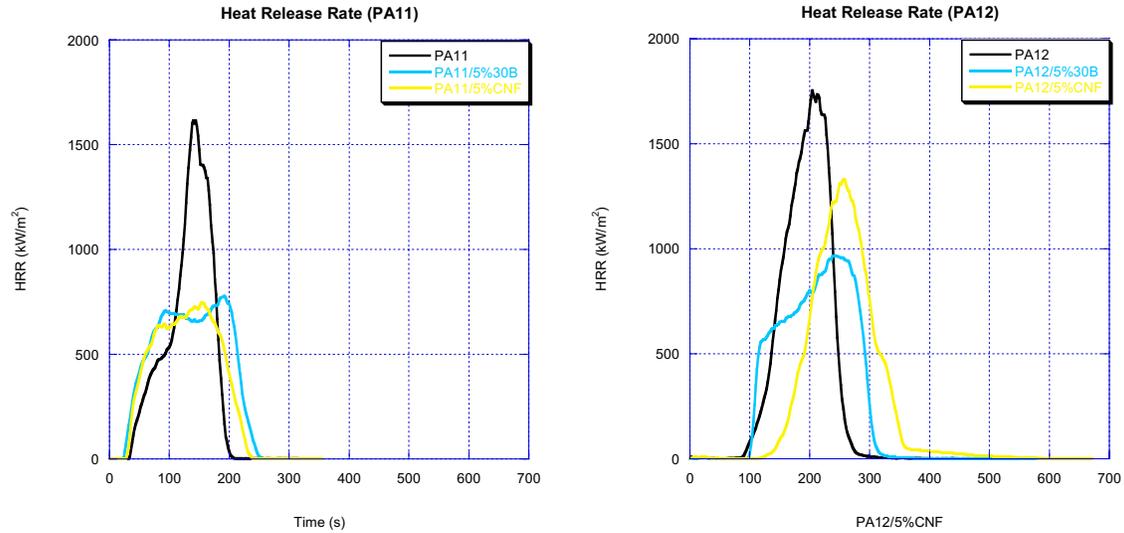
Figure 7 Heat release rate of PA11N (left) and PA12N (right).

The ideal case for the best candidate is to have minimum values of heat release rate, carbon monoxide emission, and smoke extinction coefficient, but the highest residual mass percentage. In terms of heat release rate (Figure 7), PA12-5% 30B has the lowest peak heat release rate (PHRR) as compared to the other specimens: 35% of PA12-5% CNF and 75% of PA12 baseline. PA11Ns have lower heat release rate than PA12Ns, as a result PA11Ns are more FR effective than PA12Ns.
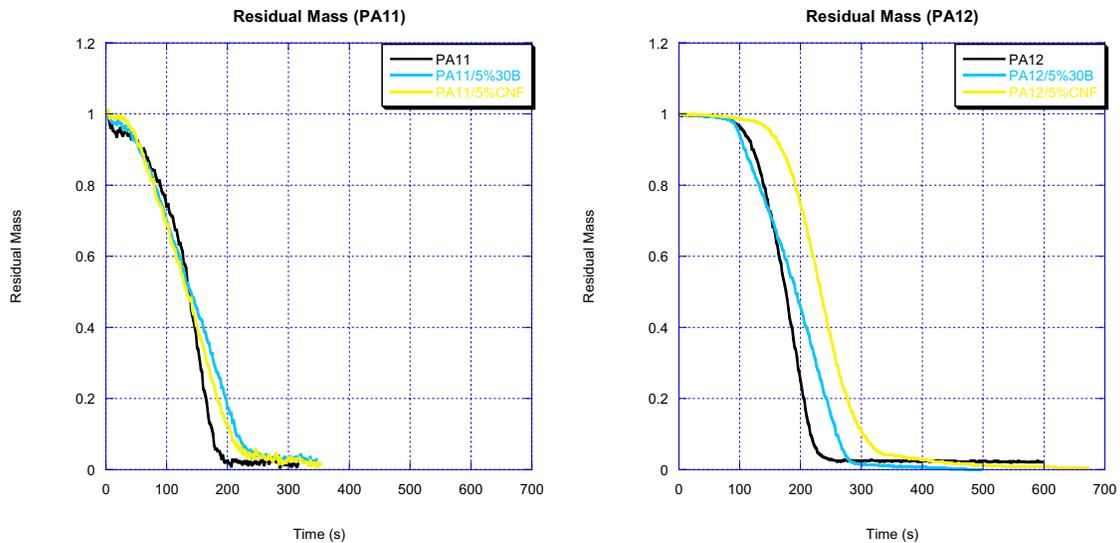
Figure 8 Residual mass of PA11N (left) and PA12N (right).

However, PA12-5% CNF produces the least smoke (Figure 10) and achieves a higher residual mass (Figure 8) during the experiment. For carbon monoxide emission (Figure 9), PA12 baseline emits the most carbon monoxide (~300 ppm) for the duration of the experiment while PA12-5% 30B and PA12-5% CNF only emit up to 60% of that for PA12 baseline. However, the time interval that PA12-5% 30B emits CO is much shorter than PA12-5% CNF.
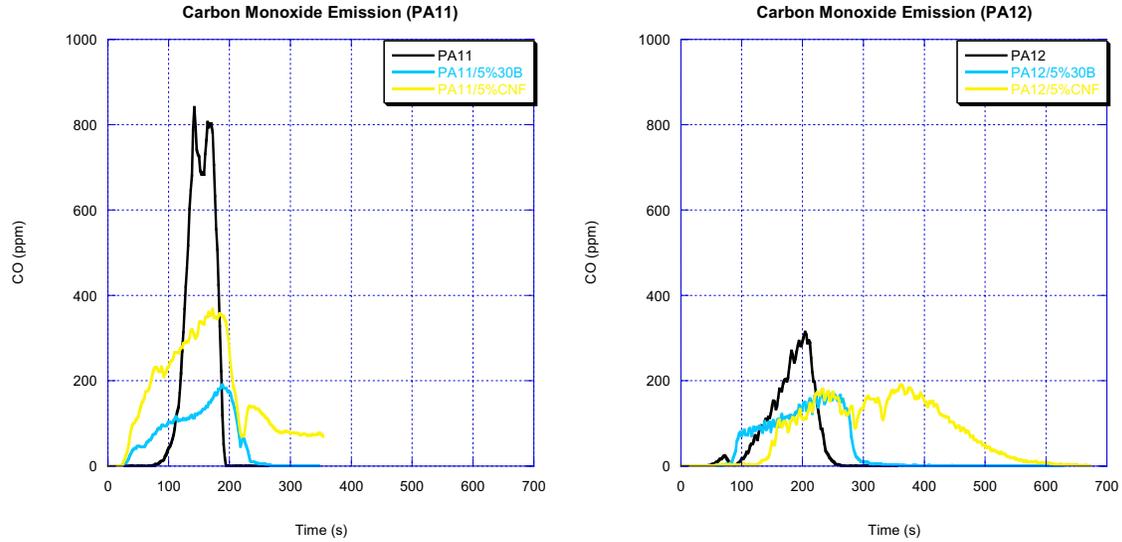
Figure 9 Carbon monoxide emission of PA11N (left) and PA12N (right).

Comparing the PA11 baseline and the PA11N with the same weight loading of clay and carbon nanofiber, PA12 baseline and PA12N have lower carbon monoxide emission (Figure 8), produce much less smoke (Figure 10), and give a higher residual mass (Figure 8). However, the time intervals of PA12 and PA12N for peak heat release, carbon monoxide emission, and smoke extinction coefficient are at least 100s longer.
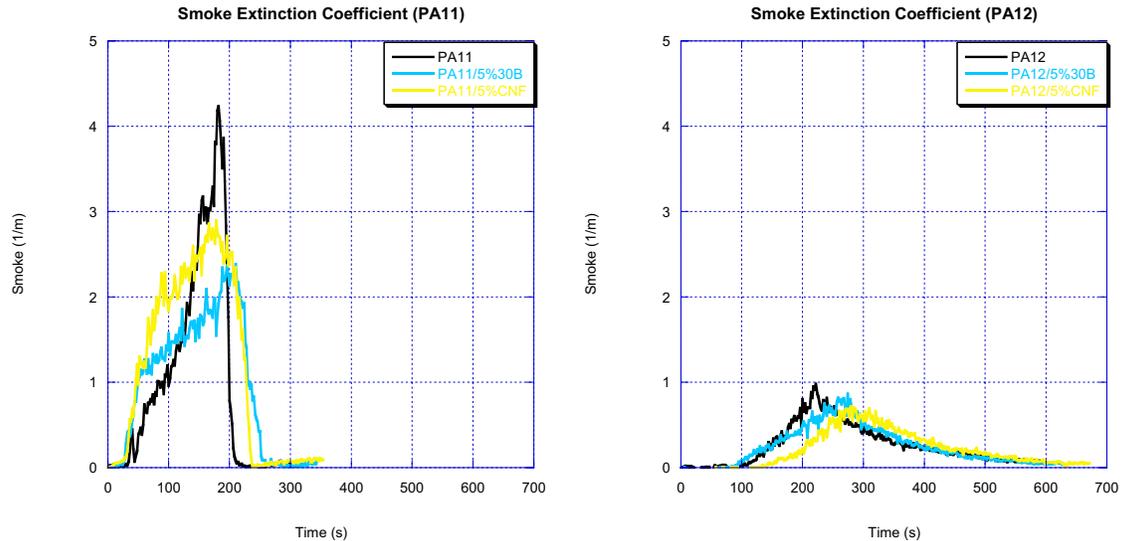
Figure 10 Smoke extinction coefficient of PA11N (left) and PA12N (right).

3.3 Mechanical Properties of Resin/Nanoparticle Systems

Tensile strength, flexural strength, Young's modulus, and elongation at break of all the PA12N are shown in Figures 11 through 14, respectively. Similar to PA11N, the tensile yield strength, flexural strength, and the Young's modulus of the polyamide 12 materials were generally enhanced by both the nanoclay and carbon nanofibers, while the elongation was significantly reduced by the addition of nanoparticles. In general, the performance of the tensile strength, flexural strength, and the Young's modulus was

enhanced with increase amount of clays, while the elongation decreased as the amount of nanoparticles increased. One exception shown by Figure 12 is the PA12-2.5% Cloisite® 30B nanocomposite. The flexural strength of that particular formulation was shown to possess better properties than the neat polyamide 12 resin. The error might be due to the material processing as voids were observed in the samples of that formulation. Statistical deviation of the flexural strength and elongation data of the PA12-2.5% Cloisite ® 30B nanocomposite was very large [27]. Further verification with a new set of a well-processed void free sample is needed.
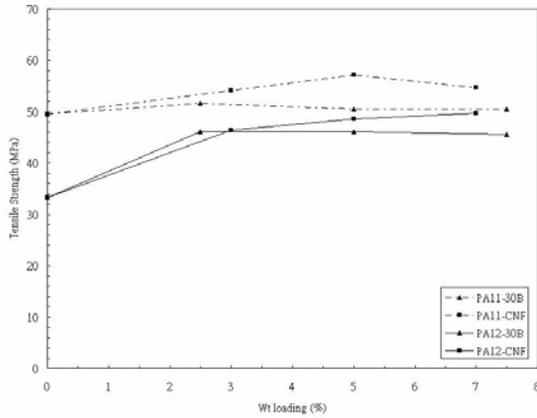
Tensile yield strength
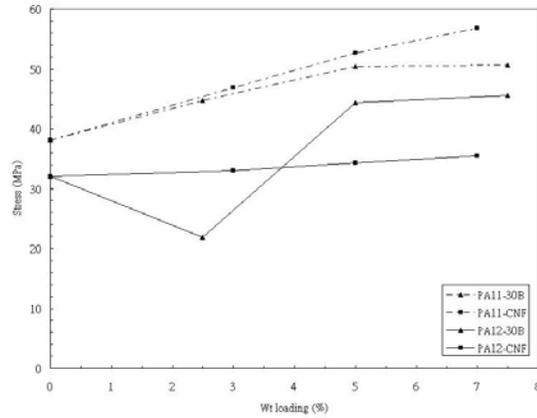
Flexural strength

Figures 11 and 12 Tensile yield strength (left) and flexural strength (right) of polyamide 11 nanocomposites and polyamide 12 nanocomposites.
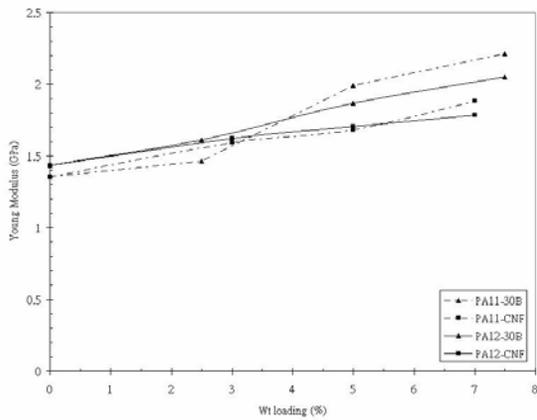
Young's modulus
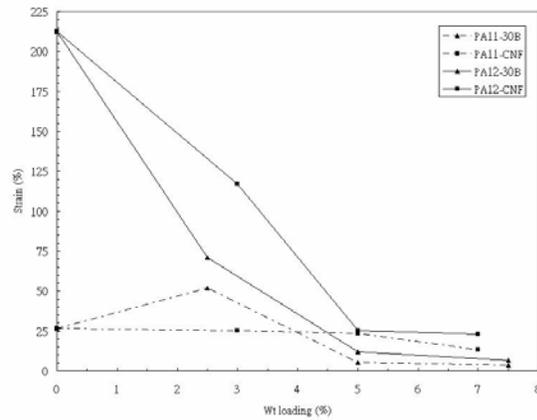
Elongation at break

Figures 13 and 14 Young's modulus (left) and elongation at break (right) of polyamide 11 nanocomposites and polyamide 12 nancomposites.

3.4 SEM Analyses of Burnt Polyamide 11 Nanocomposites

The surface and cross section of the burnt specimens were investigated by studying the mechanisms of flame retardancy. A thin layer of coating was applied to prevent charging of the nanoparticles. At 74 seconds (Figure 7) or the first peak heat release rate (the images of the burnt sample of polyamide 11 with Cloisite® 30B), large portions of

char yielded in the polymer matrix and the matrix remained uniform (Figure 19). The nanoparticles reinforced the fragile polymer char and formed a protective layer on the surface [25] that blocks the thermal wave from penetrating down the surface. On the other hand, the sample with CNF exhibited voids and discontinuous char formation on the surface (Figure 20). The char was fragile and appeared to burn throughout the matrix. The white spots on the images are presumed to be the remaining polymer matrix and suggest that the sample burnt randomly at different locations. As the length of the CNF is measured under higher magnification, it clearly shows that the usual lengths of CNF are about 0.2 microns in length. The CNF was reduced in length due to extrusion.
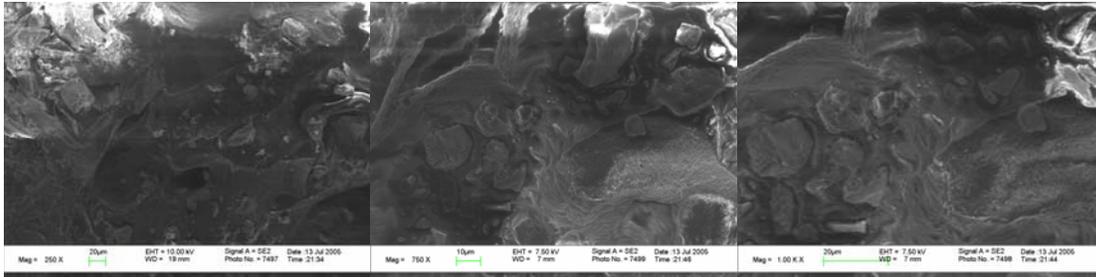
Figure 19 SEM images of post-test cone calorimeter PA11/5% Cloisite® 30B surface at the first peaked heat release rate (74 seconds) at magnifications of 250X (left), 750X (middle), and 1,000X (right).
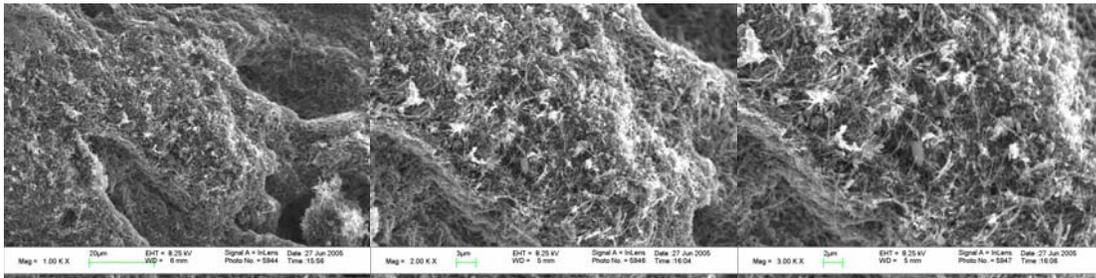
Figure 20 SEM images of post-test cone calorimeter PA11/5% PR-19-PS CNF surface at the first peaked heat release rate (74 seconds) at magnifications of 1,000X (left), 2,000X (middle), and 3,000X (right).

At the second peaked heat release rate (150s, see Figure 7), the surface of the Cloisite® 30B sample was mainly covered with char. The polymer matrix was thinned due to the loss in mass but remains uniform as opposed to the sample with carbon nanofibers, where in the matrix could not be seen at all under SEM and all that remains is nanofibers (Figures 21 and 22). It is evident that the role of the nanoclay is to reduce the heat release rate by forming an insulating char structure on the surface of the polymer matrix . The nanoclay facilitated the formation of a heat shield to prevent the polymer matrix from burning as it was below the char surface.
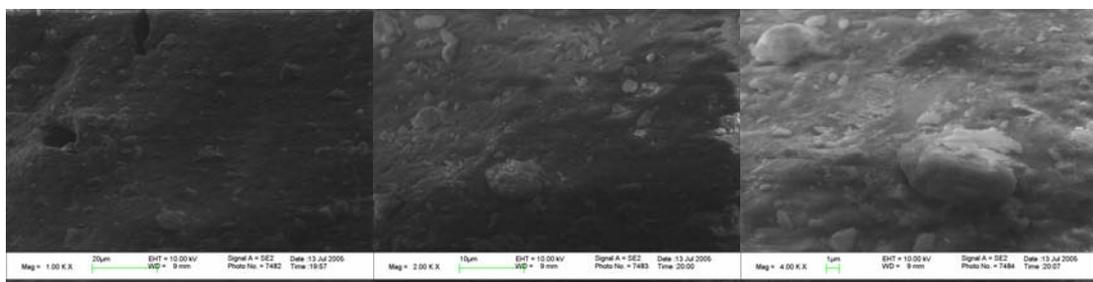
Figure 21 SEM images of post-test cone calorimeter PA11/5% Cloisite 30B surface at the second peaked heat release rate (150 seconds) at magnifications of 1,000X (left), 2,000X (middle), and 4,000X (right).
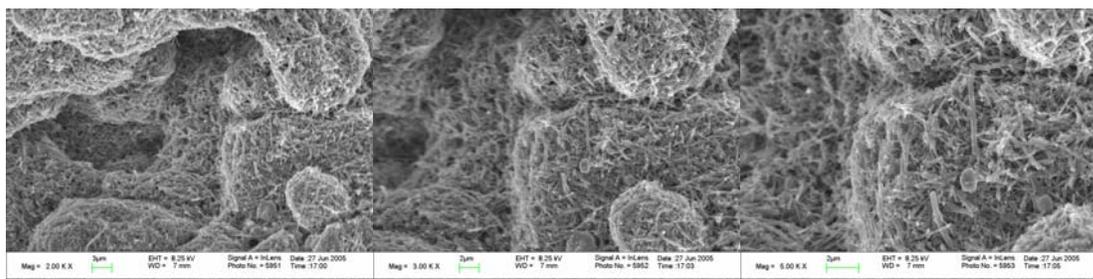
Figure 22 SEM images of post-test cone calorimeter PA11/5% PR-19-PS CNF surface at the second peaked heat release rate (150 seconds) at magnifications of 2,000X (left), 3,000X (middle), and 5,000X (right).

3.5 SLS Processing of Polyamide 11 Nanocomposites

Based on the thermal, mechanical, and flammability properties of the injection molded PA11 nanocomposite specimens, the PA11 (control) and four PA11 nanocomposite pellets were transformed into fine SLS powders. Fifty pounds of the following PA11 formulations were cryogenically ground into μm-sized powder using Vortec Products Company's proprietary conditions:

- PA11 (control)
- PA11/5 wt% Cloisite 30B nanoclay
- PA11/5 wt% Cloisite 93A nanoclay
- PA11/5 wt% PR-19-PS CNFs
- PA11/7 wt% PR-19-PS CNFs

Particle Size Analysis The average mean particle size of these five SLS powders was about 68 μm. The particle size distribution (PSD) measured by the Microtrac particle analyzer of PA11/30B and PA11-CNF are shown in Figures 23 *(a)* and 23 *(b)*, respectively. The average mean particle diameters of the PA11/Cloisite 30B and PA11/Cloisite 93A were about 68 μm while the PA11/PR-19-PS CNF powders were in between 68 to 114 μm. The PSD of the PA11N-clay ranges from 1.4 to 249 μm while the PSD of the PA11N-CNF ranges from 7.8 to 352 μm. It is obvious that the PA11/CNF powder PSD is wider and their sizes are larger than the PA11/clay powders.

| (a) | (b) |
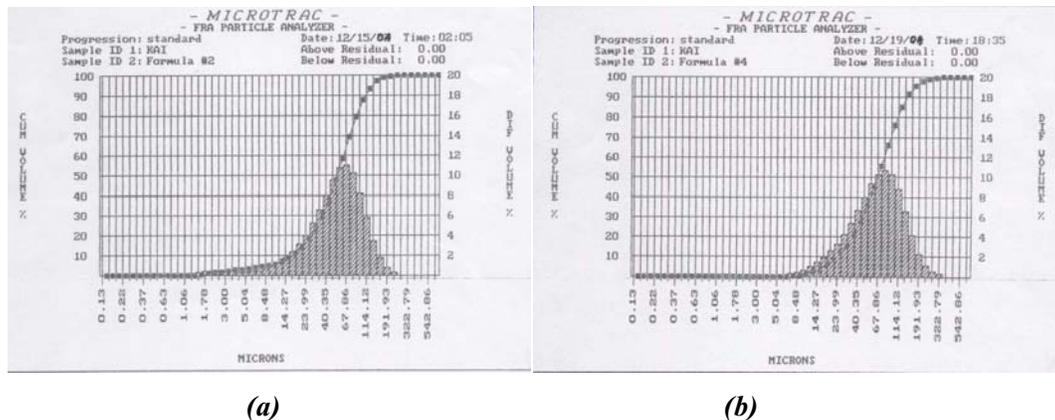
Figure 23 *(a) and (b)* Particle size distribution of the SLS powder of *(a)* PA11N-clay and *(b)* PA11N-CNF measured by Microtrac particle analyzer.

SLS Processing These SLS powders were used to fabricate SLS parts using the 3D Systems Vanguard HS machine at The University of Texas at Austin/Solid Freeform Fabrication (SFF) Manufacturing Lab. The SLS process has been proven to be successful for PA11N-CNF. It is, however, unsuccessful for PA11N-clay, thus far. The observed reason for the failure is that the process is inhibited by powder mechanics. The poor powder flow for the PA11N-clay led to poor powder deposition and subsequent SLS processing difficulties. The difference in powder mechanics can be seen visibly: the PA11N-clay flow like flour, whilst the PA11N-CNF flow like grains of fine particles. Yet, there is no quantitative measurement technique in the existing SLS field to characterize powder flow behavior. This makes it very difficult to predict the processibility of a new material a priori. It is suggested that a quantitative powder mechanics characterization methodology be developed to facilitate SLS processing [28].

At the present, only two of the five SLS candidates (PA11/5 wt% PR-19-PS CNF and PA11/7 wt% PR 19-PS CNF) were successfully fabricated into complicated SLS parts as shown in Figure 24. These are full dense SLS parts. Optimal SLS processing conditions has been achieved for these PA11N-CNF formulations. Microstructural analyses of pre- and post-test PA11N specimens were conducted on injection molded and SLS specimens in order to gain fundamental understanding of material behavior [25]. Thermal conductivity data for the PA11N-CNF are reported elsewhere [29]. Additional processing and characterization of SLS PA11N with conventional fire retardant additives are still in progress.
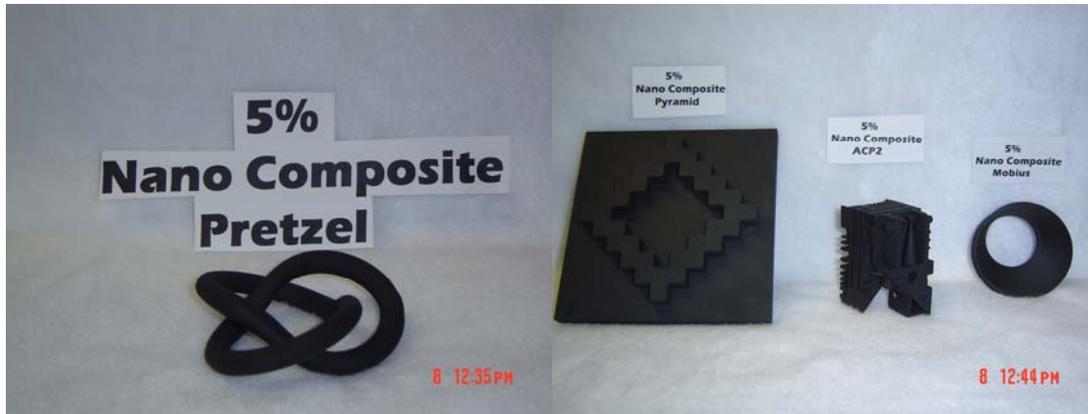
Figure 24 Polyamide 11/5% PR-19-PS CNF SLS parts.

4. SUMMARY AND CONCLUSIONS

A total of fifteen polymer blends of polyamide 11 polymer were compounded via twin screw extrusion with MMT nanoclay, nanosilica, and CNF separately. Six polymer blends of polyamide 12 polymer with MMT nanoclay and CNF were also compounded separately. Injection molded specimens of PA11, PA12, PA11N, and PA12N were fabricated for physical, mechanical, thermal, and flammability properties measurements. The results were compared with PA11 baseline, PA12 baseline, and their nanocomposites. Transmission electron microscopy (TEM) was used to examine the dispersion of the nanoparticles in the PA11 and PA12 polymers. Mechanical properties such as tensile yield strength, flexural strength, elongation at break, and Young's modulus were measured. Thermal stability was analyzed using thermogravimetric analysis. Flammability properties were measured by cone calorimeter at a radiant heat flux of 50 kW/m^2.

The following conclusions were drawn from this study:

1. The TEM analyses have shown that good dispersions of the nanoclays and carbon nanofibers in the polyamide 11 and 12 resin systems were achieved.
2. Nanosilica did not uniformly disperse into PA11 and was not examined with PA12.
3. Thermal stability of the polyamide 12 was enhanced by the nanoclay while the carbon nanofibers had little or no effect on polyamide 12.
4. The flammability properties, namely heat release rate, carbon monoxide emission, and smoke extinction coefficient, of the polyamide 11 and 12 were enhanced by the addition of nanoclays and carbon nanofibers.
5. Compared with PA11N, PA12N has lower carbon monoxide emission and smoke extinction coefficient, but higher residual mass. However, PA12N burned about 100s longer.
6. Both nanoparticles had little or no effect on the hardness of PA11 and PA12 polymers.
7. Subtle features of using nanoclay or CNFs as nanomaterial in PA12N and PA11N indicate that CNF provided the highest tensile yield strength whereas the nanoclay provided enhanced modulus with increasing amount of nanoclay. The nanoclay

provided the PA12N with higher flexural strength than the CNF, while the CNF gave a higher flexural strength value in PA11N.

8. In general, the elongation at break for both the PA11N and PA12N was decreased by both the nanoclay and CNF.
9. The PA11N-CNF specimens have wider particle size distribution and larger particle size than the PA11N-clay specimens.
10. Fabrication of fully dense, complicated PA11/5 wt% PR-19-PS CNF and PA11/7 wt% PR-19-PS CNF SLS parts were successfully demonstrated.

5. REFERENCES

1. *Fire and Polymers III. Materials and Solutions for Hazard Prevention*, G. N. Nelson and C. A. Wilke, Ed., American Chemical Society, Washington, D.C., 2001.
2. E. Giannelis, *Adv. Mater*. 8, 29 (1996).
3. J. W. Gilman, T. Kashiwagi, *SAMPE J.,* 33 (4), 40 (1997).
4. J. W. Gilman, *Appl. Clay. Sci.* 15, 31 (1999).
5. J. Zhu, A. B. Morgan, J. Lamelas, C. A. Wilke, *Chem. Mater.* 13, 3774 (2001).
6. M. Zanetti, G. Camino, R. Mulhaupt, *Polym. Degrad. Stabil.* 74, 413 (2001).
7. J. W. Gilman, C. L. Jackson, A. B. Morgan, R. Harris, Jr., E. Manias, E. P. Giannelis, M. Wuthernow, D. Hilton, S. H. Phillips, *Chem. Mater*. 12, 1866 (2000).
8. T. Kashiwagi, E. Grulke, J. Hilding, R. Harris, W. Awad, J. Douglas, *Macromol. Rapid Commun.*, 23, 761 (2002).
9. J. H. Koo *et al.*, *Proc. SAMPE 2003*, SAMPE, Covina, CA, 2003, p. 954.
10. F. Yang, R. A. Yngard, G. L. Nelson, "Nanocomposites 2002," San Diego, CA, Sept 23-5, 2002.
11. T. Kashiwagi *et al.*, "Nanocomposites 2002," San Diego, CA, Sept 23-25, 2002.
12. A. D. Pool and H. T. Hahn, *Proc. SAMPE 2003*, SAMPE, Covina, CA, 2003.
13. T. D. Fornes and D. R. Paul, *Macromolecules*, 37, 7698 (2004).
14. Polyamide 11 technical data sheet, Arkema, Inc.
15. Polyamide 12 technical data sheet, Degussa, AG.
16. J. H. Koo, *Polymer Nanocomposites: Processing, Characterization, and Applications*, New York, 2006, pp. 9-49.
17. Cloisite® 30B technical data sheet, Southern Clay Products, Gonzales, TX.
18. Cloisite® 93A technical data sheet, Southern Clay Products, Gonzales, TX.
19. Technical Bulletin AEROSIL® No. 27, Degussa AG, D-63403 Hanau-Wolfgang, Germany, 10/2001.
20. AEROSIL® R805 technical data sheet, Degussa AG, D-63403 Hanau-Wolfgang, Germany.
21. AEROSIL® R202 technical data sheet, Degussa AG, D-63403 Hanau-Wolfgang, Germany.
22. M.L. Lake, J-M. Ting. In *Carbon Materials for Advanced Technologies*, T.D. Burchell, Ed., Pergamon, Oxford: England, 1999.
23. M.L. Lake, manuscript from Applied Sciences, Inc., Cedarville, OH, 11/2002.
24. B. Maruyama and K. Alam, *SAMPE J.*, 38 (3), 59 (2002).

25. J. H. Koo, S. Lao *et al.*, "Microstructural Analyses of Nylon 11 Nanocomposites," *Proc. SAMPE 2005 ISTC*, SAMPE, Covina, CA (2005).
26. J. H. Koo, J. Cheng *et al.*, "Flammability and Mechanical Properties of Nylon 11 Nanocomposites," with *Proc. SAMPE 2005 Int'l Symposium*, SAMPE, Covina (2005).
27. S. Lao, J. H. Koo *et al.*, "Flammability and Mechanical Properties of Nylon 12 Nanocomposites," with *Proc. SAMPE 2006 Int'l Symposium*, SAMPE, Covina (2006).
28. J. Cheng, S. Lao, K. Nguyen, D. Ho, T. Cummings, and J.H. Koo, "SLS Processing of Nylon 11 Nanocomposites," *Proc. 17th Solid Freeform Fabrication Symposium*, The University of Texas at Austin, Austin, TX, Aug. 2005.
29. A. Cummings, L. Shi, and J.H. Koo, "Thermal Conductivity Measurements of Nylon 11-Carbon Nanofiber Nanocomposites," *Proc. of IMECE2005 (2005 ASME International Mechanical Engineering Congress & Exposition)*, Orlando, FL, Nov. 5-11, 2005.

ACKNOWLEDGEMENTS